Int J Adv Manuf Technol (2016) 87:2841–2851
DOI 10.1007/s00170-016-8670-9

ORIGINAL ARTICLE

Numerical investigation of weather strip extrusion forming process by thermal flow analysis

J. R. Cho[1] · **J. H. Choi**[2]

Received: 18 November 2015 / Accepted: 23 March 2016 / Published online: 5 April 2016

Abstract The weather strip used to protect the interiors of vehicles from rainwater, dust, and noise is manufactured through the special extrusion forming process in which the solid-state rubber material is forced to be compressed, melted, and extruded out through the forming die. The extrusion forming process is characterized by the thermal flow of melted rubber material, which is in turn influenced by the slip condition at the inner wall of the head and the shear viscosity as well as the flow vorticity. The die design, which substantially affects the extrusion forming quality, is made based on the thermal flow characteristics, particularly in the head region. In this context, this paper is concerned with the numerical investigation of thermal flow characteristics in the head region by the finite element analysis. The flow profile, streamlines, and the temperature distribution are investigated with respect to the breaker plate, wall slip condition, and the shear viscosity model. The extrusion forming using twin dies is investigated as well with respect to the imbalance of the wall temperature and inlet flow velocity.

Keywords Weather strip · Extrusion forming process · Thermal flow analysis · Power-law shear viscosity model · Flow velocity · Process temperature · Twin dies

✉ J. R. Cho
jrcho@hongik.ac.kr

[1] Naval Architecture and Ocean Engineering, Hongik University, Sejong 339-701, Korea

[2] Graduate School of Mechanical System, Pusan National University, Busan 609-735, Korea

Nomenclature

Ω	Flow domain in the head region
$\partial\Omega$	Boundary of flow domain
$\partial\Omega_F$	Free surface contacting with surrounding air
$\partial\Omega_C$	Inlet and the cutting surface
$\partial\Omega_I$	Interfaces with breaker plate head wall and die
μ	Shear viscosity of melted rubber flow
γ	Shear rate
K	Consistency index
n	Flow behavior index
T	Temperature
$\boldsymbol{v}$	Flow velocity
ρ	Mass density
σ	Stress
e	Strain
$\boldsymbol{f}$	Body force
p	Hydrodynamic pressure
Φ	Viscous dissipation function
Q_H	Heat generation
C_V	Volumetric specific heat
κ	Thermal conductivity
h_C	Convection coefficient
q_f	Frictional heat
$\boldsymbol{t}_f$	Frictional force
$\mathbf{v}_s$	Sliding velocity

T_0 Reference temperature
k Material-dependent parameter
T_{air} Air temperature
$\hat{T}$ Flow temperature at inlet

1 Introduction

A weather strip is a long flexible rubber product having the particular hollow cross-section that is assembled along the door edge of various vehicles, such as automotive and vessel [1, 2]. It is used to protect the interior space of a vehicle from rainwater, external dust, and sound, and furthermore, it absorbs the structural vibration of the vehicle to some extent [3]. Both the cross-sectional shape and the overall size depend on the vehicle model and the cross-sectional configuration of the fitting region where the weather strip is inserted. Nevertheless, the common requirement of weather strips is the dimension precision not only for the tight fit into the installation slot but also for securing the designed contact performance. Furthermore, a weather strip is forced to be compressed when door is closed and to be relaxed when door is opened. Thus, the security of structural durability against the frequent shutting/opening operations of door is desired up to at least the life span of vehicle [1].

It is manufactured with solid-state raw rubber material by the specially designed extrusion forming machine [4] in which raw rubber material undergoes the phase change from the solid state to the melted liquid state by the friction-induced heat source. As will be shown later, the raw rubber material is to be fed and compressed by the rotating screw, and furthermore, it is to be melted by the frictional slip between chamber and compressor. One of apparent features of melted rubber flow is the occurrence of vorticity while rubber material is passing through the spiral-type compressor. Since the vortex flow gives rise to the bad effect on the extrusion forming quality, a metallic disc having a number of holes, called by breaker plate [5], is placed at the inlet of the head to suppress the vortex flow.

The field experiments reported that the product quality is strongly influenced by the stabilization and uniformity of the melted rubber flow, particularly in the head region. In other words, the characteristic analysis of thermal flow is essential for the optimum design of extrusion dies [6, 7]. Nevertheless, the design of an extrusion forming die has been made through a trial and error approach [8]. In this context, we intend to investigate in this paper the thermal flow characteristics in the extrusion forming process of weather strip, particularly in the head region composed of die, breaker plate and nozzle-type chamber. Besides the beaker plate, the melted rubber flow is also influenced by the slip condition at the inner surface of chamber and the shear viscosity of rubber flow. The melted rubber flow exhibits the non-Newtonian behavior so that its shear viscosity varies with the temperature and shear strain [9]. Hence, the thermal flow characteristics such as the flow velocity, streamline and temperature are numerically investigated with respect to the slip condition, the viscosity model and the inlet flow velocity. As well, the effects of imbalance of the wall temperature and the inlet flow velocity on the thermal flow characteristics are investigated, particularly for twin dies that is under study to increase the production capacity.

Fig. 1 **a** Weather strips used for vehicles, **b** real forming scene

2 Problem description

2.1 Extrusion forming process of weather strip

Referring to Fig. 1a, the type of weather strip is characterized by its cross-sectional shape, which is in turn determined by the geometric configuration and dimension of opening and shutting region of vehicle where it is to be fitted. In other words, both the overall size and the cross-sectional shape vary depending on the vehicle model and the fitting location. The original product extruded from the forming machine is ultra-long seamless, as represented in Fig. 1b, and it is to be cut into a number of pieces having the equal length which is determined by the edge length of vehicle door.

Referring to Fig. 2, the extrusion forming process is divided into feeding, compressing and head regions. In the feeding and compressing regions, the raw rubber material is forced to be fed and compressed by the rotating spiral-type compressor and melted by the friction-induced heat generation between

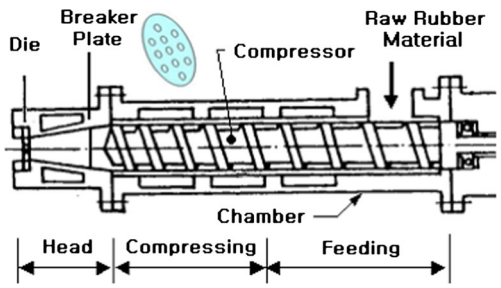

Fig. 2 Extrusion forming process of weather strip [4]

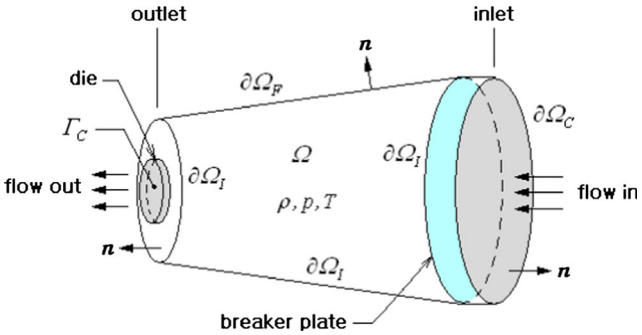

Fig. 3 Domain definition for the thermal flow analysis

the rubber and the inner chamber wall. The compressor revolution-induced vorticity in the melted rubber flow is suppressed by the breaker plate which is a disc-type metallic filter having a number of holes. In the head region, the laminar rubber flow is pushed into the forming die and extruded out with the help of the external tension that is transferred through the endless extruded product ahead.

2.2 Steady-state non-Newtonian thermal flow

The extrusion forming of weather strip is a steady-state process, except for the initial short time period for stabilizing the process. Thus, the current study focuses on the steady-state thermal flow characteristics in the head region. Restricting to the rubber flow between the breaker plate and the die front, as depicted in Fig. 3, we denote Ω be the problem domain with boundary $\partial\Omega = \overline{\partial\Omega_C \cup \partial\Omega_I \cup \partial\Omega_F}$. Here, $\partial\Omega_C$ denotes the inlet and cutting surface Γ_C of the restricted domain, $\partial\Omega_I$ the common interfaces with the breaker plate, head wall and die, and $\partial\Omega_F$ the free surface contacting with surrounding air.

Assuming that the thermal flow is incompressible and non-Newtonian and employing the Eulerian kinematic description [4], the steady-state flow velocity $\boldsymbol{v}(\boldsymbol{x})$ is governed by the continuity equation

$$\nabla\cdot v = 0, \quad \text{in} \quad \Omega \tag{1}$$

and the momentum equations

$$\rho(v\cdot\nabla)v = \nabla\cdot\sigma + \rho f, \quad in \quad \Omega \tag{2}$$

with the boundary conditions

$$v(x) = \hat{v}(x), \quad \text{on} \quad \partial\Omega_C \tag{3}$$

$$v(x)\cdot n = 0, \quad \text{on} \quad \partial\Omega_I \tag{4}$$

In which, ρ is the mass density, $\boldsymbol{f}$ the body force, $\boldsymbol{n}$ the outward unit normal vector. In incompressible flow, the stress tensor σ_{ij} is constituted with the strain-rate tensor $e_{ij}=(v_{i,j}+v_{j,i})/2$ as $\sigma_{ij}=-p\delta_{ij}+2\mu e_{ij}$ with the hydrostatic pressure p and the shear viscosity μ.

On the other hand, the steady-state temperature field $T(\boldsymbol{x})$ of the rubber flow is governed by the energy equation

$$\rho C_V(\mathbf{v}\cdot\nabla)T - \nabla\cdot(\kappa\nabla T) = Q_H + \Phi \tag{5}$$

with the boundary conditions

$$T(x) = \hat{T}(x), \quad on \quad \partial\Omega_C\backslash\Gamma_C \tag{6}$$

$$-\kappa\nabla T\cdot n = q_f\left(=|t_f||v_s|\right), \quad on \quad \partial\Omega_I \tag{7}$$

$$-\kappa\nabla T\cdot n = h_C(T - T_{air}), \quad on \quad \partial\Omega_F\cup\Gamma_C \tag{8}$$

Where, Q_H denotes the heat generation and the viscous dissipation Φ is defined by $\Phi=2\mu e_{ij}e_{ij}$. On the other hand, C_V is the specific heat at constant volume; κ the thermal conductivity, q_f the frictional heat induced by the frictional force $\boldsymbol{t}_f$ and the sliding velocity $\boldsymbol{v}_s$, h_C the convection coefficient [5], and $\hat{T}$ the flow temperature at inlet. The frictional force $\boldsymbol{t}_f$ is calculated by the generalized Navier's law such that $\boldsymbol{t}_f=k\boldsymbol{v}_s$ with the material-dependent parameter k.

3 Shear viscosity in function of temperature and shear strain

3.1 Power-law shear viscosity model

Referring to Fig. 4, fluids can be generally classified into Newtonian and non-Newtonian, but in reality all the fluids exhibit the non-Newtonian behavior. Differing from Newtonian fluid showing the linear relationship between shear rate and shear stress, non-Newtonian fluids display the

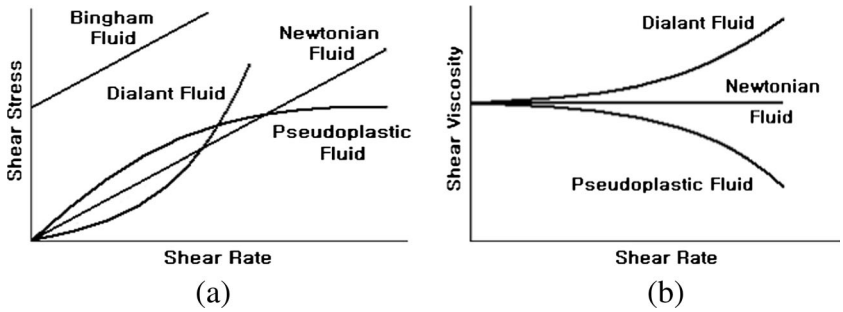

Fig. 4 Newtonian and non-Newtonian fluids: **a**shear stress versus shear rate, **b** shear viscosity versus shear rate

Table 1 The measured shear viscosities at the shear strain rate of 10

Temperature (°C)	60	70	80	90	100	110	120
Shear viscosity $\times 10^3$ (m^2/s)	8.44	7.05	6.03	4.84	4.17	3.62	3.06

Table 2 The consistency indices K determined from the μ–γ plots

Temperature T(°C)	60	80	100	120
Values of K	31,194.06	11,186.86	7085.18	5729.0

nonlinear relationship and their apparent viscosities are varying with shear rate. As shown in Fig. 4a, non-Newtonian fluids are divided into dialant (shear hardening), pseudoplastic (shear thinning), and bingham. The shear viscosity of shear hardening fluid increases in proportional to shear rate, and vice versa for shear thinning fluid. Meanwhile, bingham fluid exhibits the same linear relationship between shear rate and shear stress as Newtonian fluid, but it does not produce shear rate until its shear stress reaches the specific level.

Most of high molecular substances such as elastomer exhibit the shear thinning characteristic, and the melted rubber material in the extrusion forming process of weather strip does also belong to this category. Meanwhile, the apparent viscosities shown in Fig. 4b of three kinds of fluids can be represented by a generalized power-law material model expressed by [9, 10]

$$\mu = K(T)\dot{\gamma}^{n(T)-1} \tag{9}$$

Where, $\dot{\gamma}$ is the shear strain rate, K the temperature-dependent consistency index, and n the temperature-dependent flow behavior index, respectively. Depending on the value of n, fluids are characterized as follows: $n=1$ for Newtonian, $n<1$ for shear thinning, and $n>1$ for shear thickening. And, two indices K and n are in turn expressed by

$$K = K_0 \exp\left(-A \times \left[\frac{T-T_0}{T_0}\right]\right) \tag{10}$$

$$n = n_0 + B\left(\frac{T-T_0}{T_0}\right) \tag{11}$$

in terms of temperature. Here, four parameters K_0, n_0, A and B are material-dependent constants, while T_0 indicates the reference temperature (usually, $T_0 = 320\,K$).

3.2 Interpolation of shear viscosity

The rubber material considered in this study is CMB (carbon master batch) W6033, and its kinematic viscosities at several temperatures and strain rates are available. The values in Table 1 at the shear strain rate of 10 and three plots in Fig. 5 at the temperatures of 80, 100 and 120 °C are provided from the R&D Center of Hwaseung R&A Co. Those were obtained by the ML(1 + 4) experiment method [11] in which the shear viscosity of a rubber compound specimen is measured during four minutes after heated during one minute.

We first determined two indices K and n in Eq. (9) at three temperatures of 80, 100 and 120 °C by applying the incremental scheme to the corresponding three plots in Fig. 5. It is found that the flow behavior indices n are almost equal to 0.36 for three different temperatures, which can be confirmed from the fact that the slopes of three plots in Fig. 5 are almost the same. In other words, the dependence of the index n on the temperature is negligible, implying that B in Eq. (11) is almost zero. Meanwhile, the consistency indices K are found as follows: 11,186.86 at 80 °C, 7,085.18 at 100 °C and 5,729.0 at 120 °C, respectively.

The two constants K_0 and A in Eq. (9) could be analytically determined using the values of K at 80, 100 and 120 °C, but this approach leads to the remarkable difference in K_0 and A

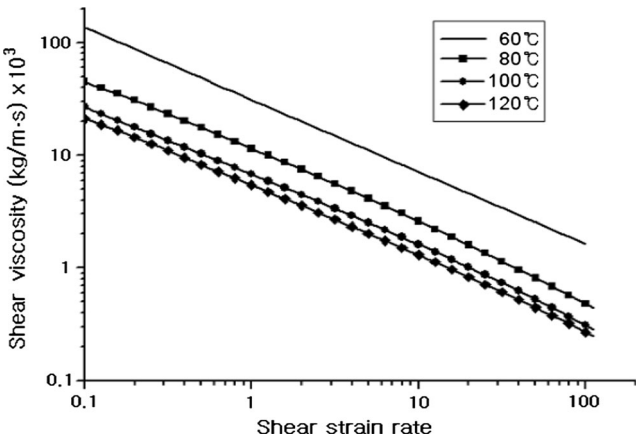

Fig. 5 Shear viscosities to the shear strain rate at different temperatures

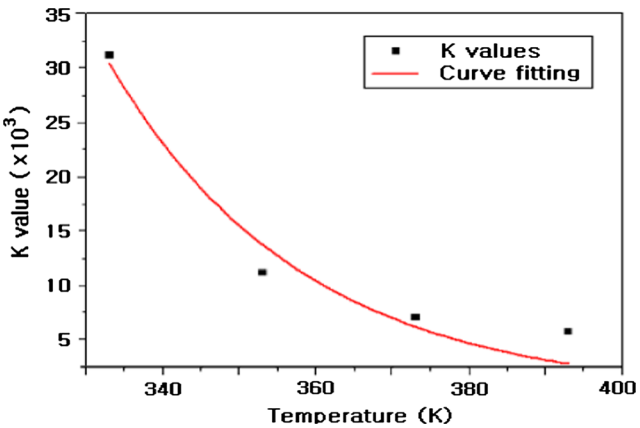

Fig. 6 Curve fitting of the consistency index K for rubber material W6033

Table 3 Material, process, and geometry data taken for the numerical experiments

Items	Data
Material & process parameters	
Mass density, $\rho(g/cm^3)$	1.18
Specific heat, $C_V(J/g \cdot K)$	2.23
Thermal conductivity, $\kappa(g \cdot cm/K \cdot s^3)$	4.0×10^4
Convection coefficient, $h_C(g/K \cdot s^3)$	9.56×10^3
Inlet temperature, $T_I(K)$	320
Inlet flow velocity, $v_x, v_r, v_\theta(cm/s)$	25, 14.4, 25
Outlet pressure, $p_o(atm)$	1.0
Major geometry data	
Inlet, outlet diameters, $D_I, D_O(cm)$	8.2, 7.0
Head length, die thickness, $L_H, t_D(cm)$	6.0, 1.0
Extrusion section size, $b_{EX} \times h_{EX}(cm)$	2.89×1.74

depending on the choice of two among three values of K. In other words, we have three equations for two unknowns. So, we take the least square method using the values of K to determine K_0 and A which are more reasonable over the wide range of temperature between 60 °C and 120 °C. To increase the accuracy of the least square method, the value K at 60 °C is also determined by applying the incremental method to the corresponding μ–γ plot at 60 °C. As shown in Fig. 5, the μ–γ plot at 60 °C was interpolated using the shear viscosity at 60 °C in Table 1 and the flow behavior index n equal to 0.36.

The consistency indices K determined from the μ–γ plots at four different temperatures are given in Table 2 and Fig. 6. By applying the least square method to these four values, we obtained the values of two constants: $K_0 = 21{,}012.82$ and $A = 6.153$, respectively. And, the final power-law model for rubber material W6033 is given by

$$\mu = 21,012,82 \cdot \exp\left(-6.153 \times \left[\frac{T-320}{320}\right]\right) \cdot \dot{\gamma}^{n-1} \tag{12}$$

with n being of 0.36. It has been found that these two values K_0 and A are positioned between the lowest and highest values

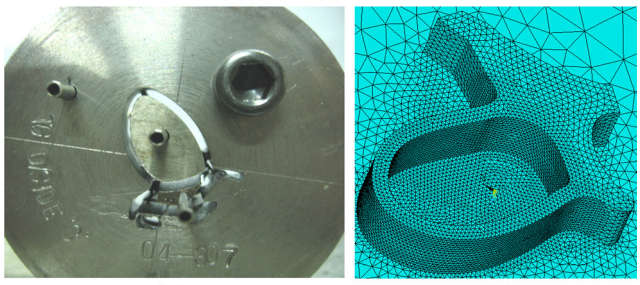

(a) (b)

Fig. 7 Extrusion die: **a** real configuration, **b** finite element mesh

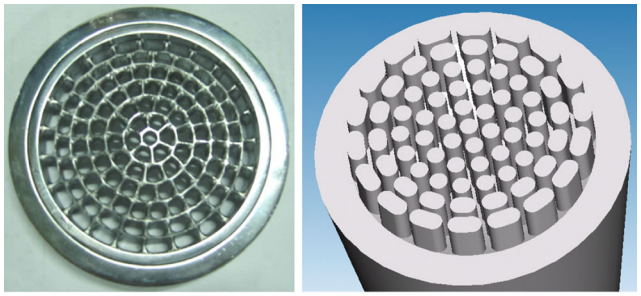

(a) (b)

Fig. 8 Breaker plate: **a** real configuration, **b** solid model

that are obtained by the above-mentioned analytical approach.

4 Numerical experiments

4.1 Finite element modeling

The major geometry dimensions of the problem domain shown in Fig. 3 are given in Table 3, where the extrusion section size indicates the maximum width and height of its cross-section. The material properties of rubber compound W6033 were provided from Hwaseung R&A, and the inlet temperature T_I was referred to the measurement data of Hwaseung R&A.

The finite element approximation of the steady-state non-Newtonian thermal flow governed by Eqs. (1)–(8) leads to the following coupled system of nonlinear equations:

$$-\mathbf{Q}^T\overline{\mathbf{v}} = 0 \tag{13}$$

$$\mathbf{C}\left(\overline{\mathbf{v}}\right)\overline{\mathbf{v}} + \mathbf{K}\overline{\mathbf{v}} - \mathbf{Q}^T\overline{\mathbf{p}} = \mathbf{F} \tag{14}$$

$$\mathbf{D}\left(\overline{\mathbf{v}}\right)\overline{\mathbf{T}} + \mathbf{L}\overline{\mathbf{T}} = \mathbf{G}\left(\overline{\mathbf{v}}\right) \tag{15}$$

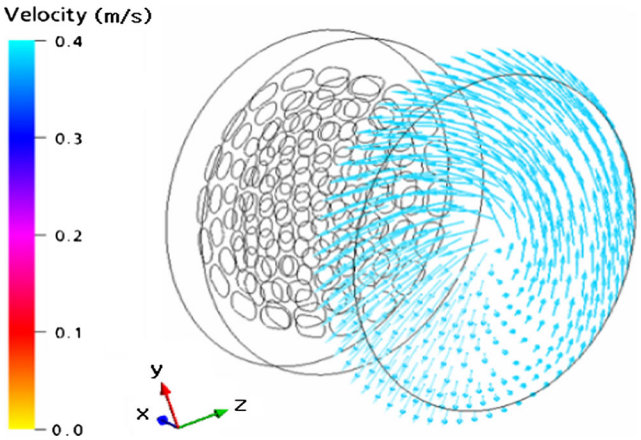

Fig. 9 Velocity profile specified at inlet

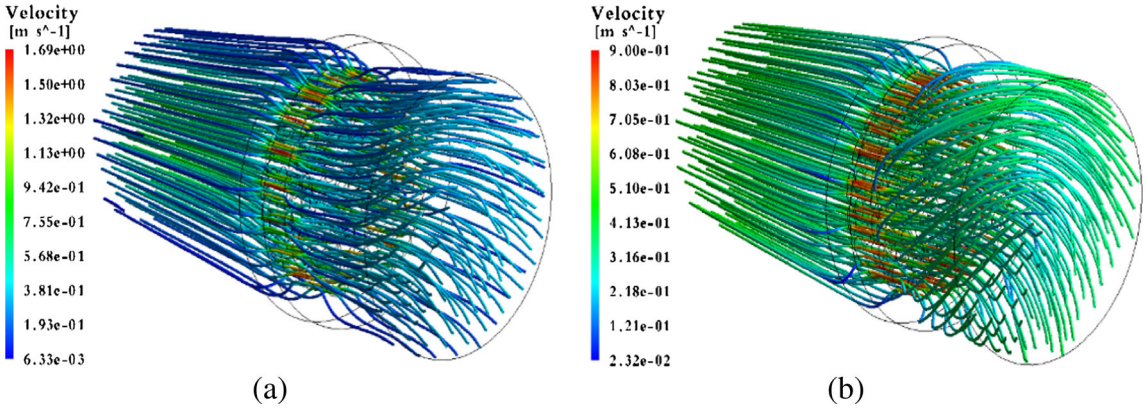

Fig. 10 Streamlines before and after breaker plate: **a** no slip, **b** free slip

The reader may refer to [4, 12] for the details on the matrices and load vectors in Eqs. (13)–(15). The velocity and pressure vectors $\{\overline{\mathbf{v}}, \overline{\mathbf{p}}\}$ are firstly solved from the coupled Eqs. (13) and (14), and then the temperature vector $\overline{\mathbf{T}}$ is solved in the staggered iterative manner. For the current study, the numerical simulation of the coupled nonlinear equations was carried out by commercial software, ANSYS CFX [13].

The head region shown in Figs. 2 and 3, including the breaker plate, die and the melted rubber flow region, was discretized with the total of 1,118,039 elements and 209,862 nodes. Figures 7 and 8 represent the real configuration of die and breaker plate and their models respectively, where the flow-passing regions were locally refined for the sake of numerical accuracy. According to the measurement at Hwaseung R&A, the temperature of melted rubber flow during the extrusion forming process is as follows: 45 ~ 50 °C in front of the breaker plate and approximately 80 °C in the head region, respectively. These experimental data will be used as the reference temperatures for the verification of numerical simulation in this study.

The inlet flow velocity $\boldsymbol{v}_I = \{v_x, v_r, v_\theta\}$ was determined based upon the diameters of chamber inner wall and compressor, the rotational speed $n = 14\,rpm$, the helix angle $\theta_H = 17.5°$ and the tread angle $\theta_T = 30°$ of the compressor. Figure 9 represents the flow profile at inlet just before the breaker plate, which is characterized by the vortex and radial flow components. Both flow components are forced to be suppressed while the rubber flow is passing through a number of cylindrical voids of the breaker plate.

4.2 Verification experiments

We first examine the flow boundary condition at the inner wall of head, for which the shear viscosity of melted rubber flow is assumed to be constant in order to avoid the highly time-consuming temperature- and shear-dependent nonlinear thermal flow analysis. Two kinds of wall conditions, no slip and free slip, are considered, and the relative difference in flow characteristics between these two wall conditions was not significantly affected by whether the shear viscosity is

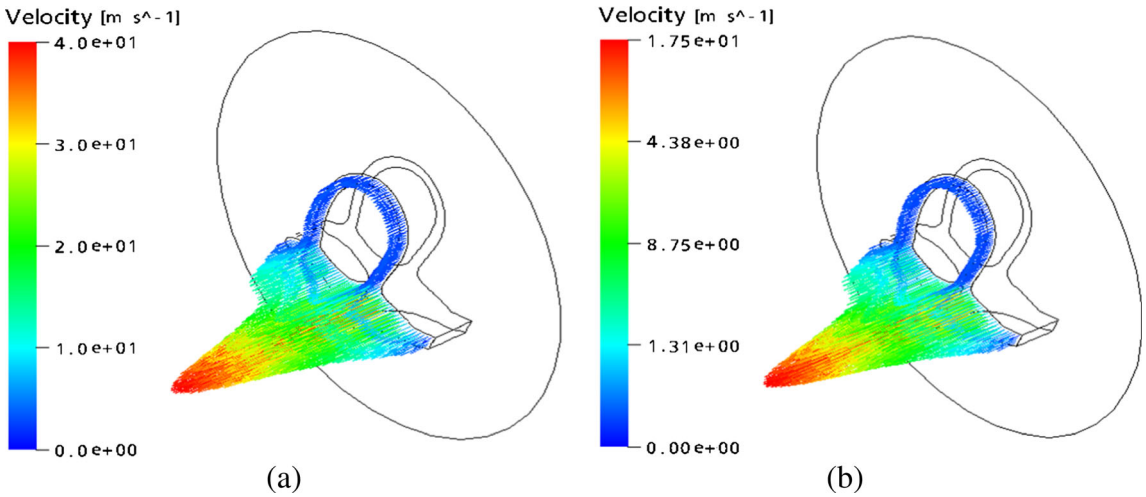

Fig. 11 Velocity profiles at die outlet: **a** no slip, **b** free slip

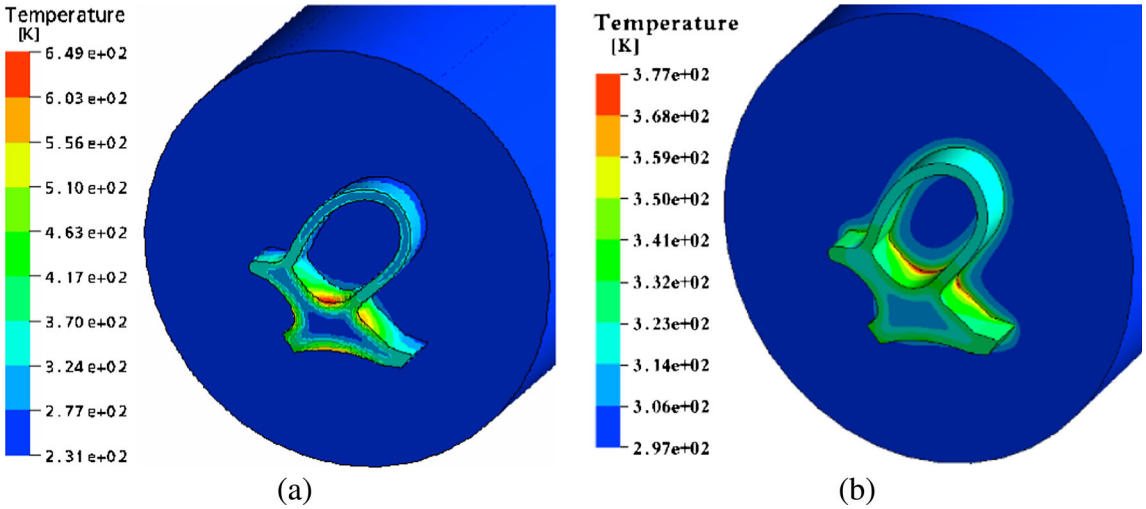

Fig. 12 Temperature distributions at die: **a** no slip, **b** free slip

temperature- and strain-dependent or not. Based on the measured peak temperature 80 °C in the head region and the averaged shear rate 10/s, a constant shear viscosity 2500 $kg/m \cdot s$ was determined using Eq. (12).

The streamlines, together with the flow velocity profiles, before and after the breaker plate are comparatively represented in Fig. 10. It is observed that the vortex is successfully suppressed by the breaker plate in both cases. But, the no slip condition shows higher velocity gradient across the flow cross-section with higher peak velocity than the free slip condition. For the no slip condition, it is of course natural to satisfy the continuity condition for the same volumetric material flow. In the real extrusion forming process, lubricant is supplied [14] to help the melted rubber flow to be smoothly extruded through chamber, breaker plate, head and forming die.

Figure 11 comparatively represents the flow profiles at die exit, where both cases show almost the same velocity profile, but, the no slip condition produces the peak flow velocity which is more than two times as high as the free slip condition. In aspect of forming quality, there is no doubt that lower velocity gradient across the die cross-section is desirable. The suitability of free slip condition can be also confirmed from the comparison of temperatures at die exit shown in Fig. 12. Owing to the excessive friction at the die wall, the no slip condition produces the abnormal temperature distribution with the maximum value close to 650 K. Considering the measured temperature about 80 °C, the peak value is more than four times as high. On the other hand, the free slip condition leads to a reasonable peak temperature so that this boundary condition seems more acceptable.

Next, the nonlinear thermal flow analysis is performed using the shear viscosity which was estimated by the power-law model given in Eq. (12). Figures 13 and 14 compare the velocity profiles and the temperature distribution at die outlet between two different shear viscosity models. When

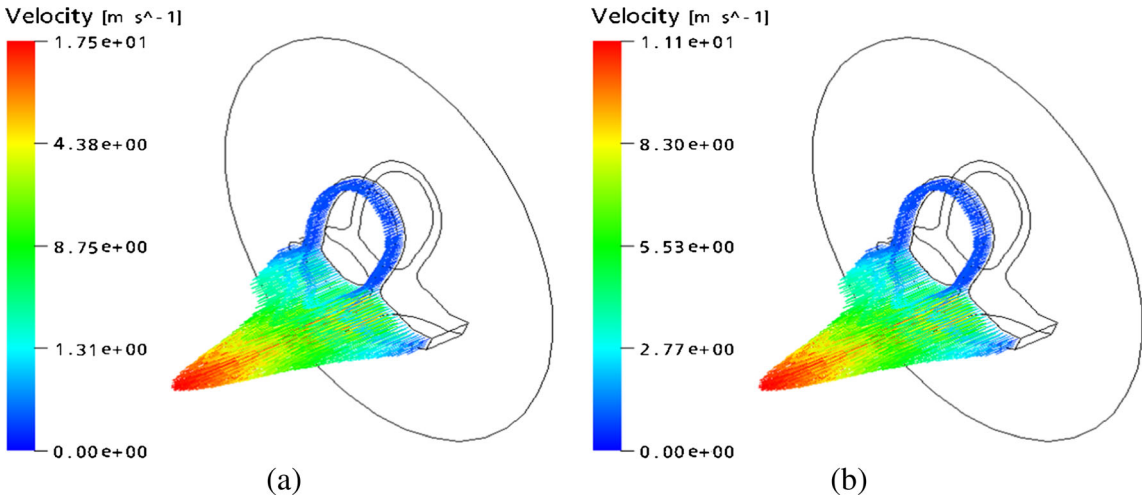

Fig. 13 Velocity profiles at die outlet: **a** constant viscosity model, **b** power-law model

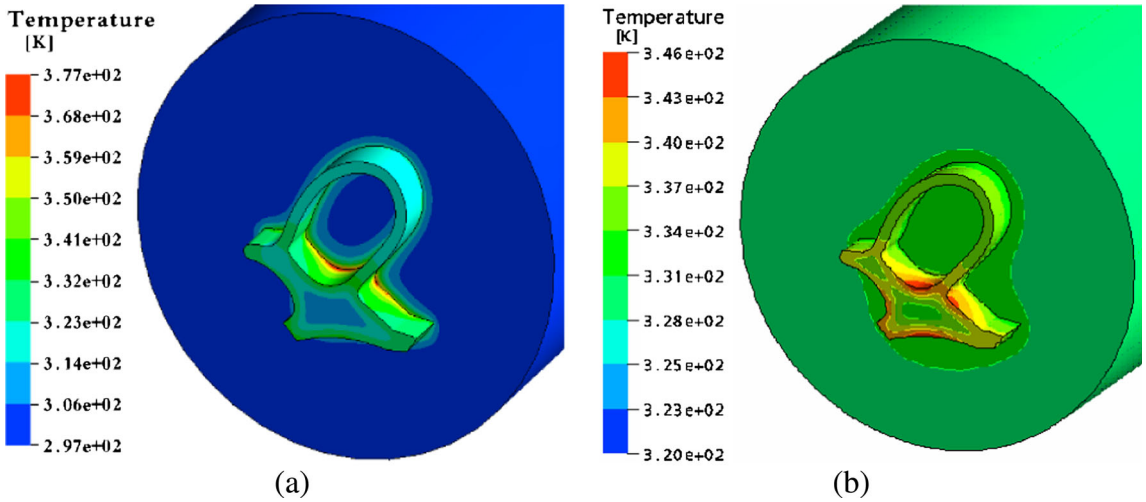

Fig. 14 Temperature distributions: **a** constant viscosity model, **b** power-law model

Table 4 Variation of the peak temperature and the peak flow velocity at die outlet to the inlet flow temperature

Inlet temperature $T_I(K)$	Peak outlet temperature (K)	Peak flow velocity at die outlet (m/s)
320	347.6	11.10
333	356.7 (2.62 %)	11.14 (0.36 %)
343	365.8 (2.55 %)	11.15 (0.09 %)

compared with the case using a constant shear viscosity, the power-law model leads to the slightly lower flow velocity and temperature. The peak velocity is reduced by 36.6 % and the maximum temperature is by 8.2 % respectively, implying that the shear viscosity is more sensitive to the flow velocity magnitude. From the fact that the shear viscosity is related to the viscous dissipation Φ in Eq. (5) and the friction at the wall, the constant shear viscosity 2500 kg/m · s is found to be set slightly higher. It was observed from Fig. 11 that the peak flow velocity is proportional to the intensity of no slip at the wall.

Furthermore, differing from the flow velocities of two cases which show almost the same profile, both cases give rise to a noticeable difference in the temperature distributions. The power-law model shows higher temperature at much more points, because the shear viscosity is determined point by point depending on the local values of temperature and shear strain. The peak temperature obtained by the power-law model is 73 °C that is more closer to the value measured at Hwaseung R&A than the value obtained using a constant shear viscosity. Thus, it has been confirmed that the power-law model is more suitable to model the shear viscosity in the real extrusion forming process.

4.3 Parametric and twin-dies experiments

The power-law model, together with the free slip condition, is applied to investigate the thermal flow characteristics with respect to the temperature value at inlet. Three different inlet

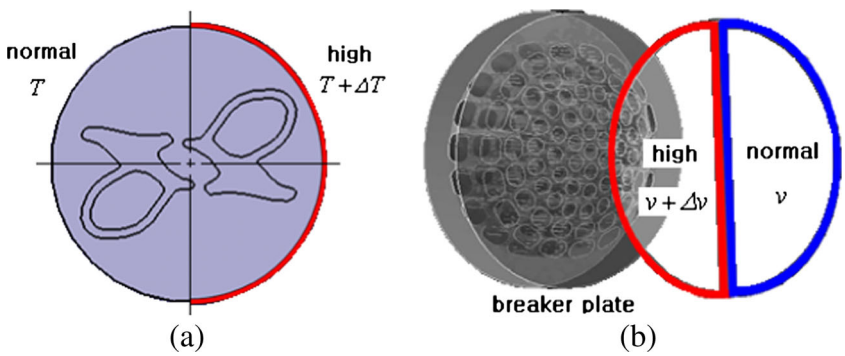

Fig. 15 Imbalance conditions: **a** temperature at the head surface, **b** flow velocity at inlet

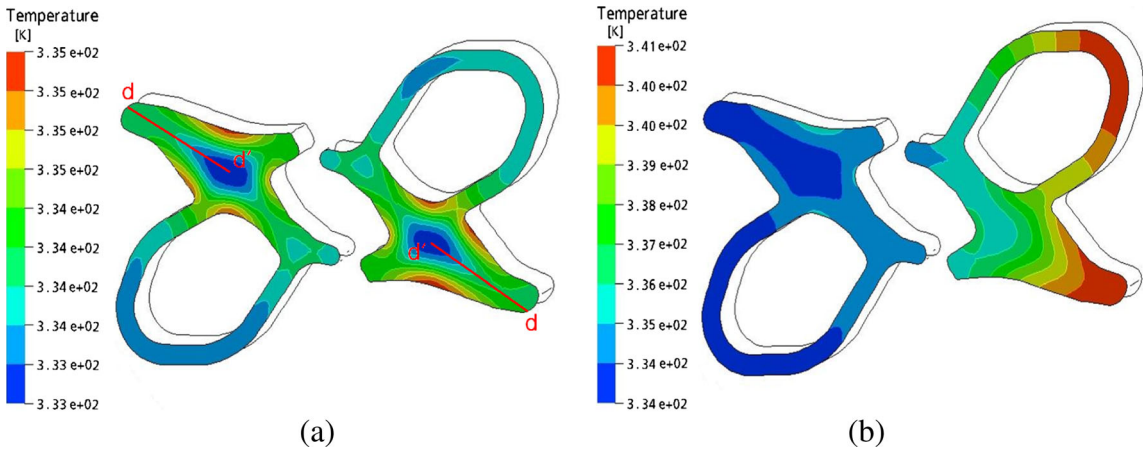

Fig. 16 Temperature distributions: **a** without temperature imbalance, **b** with temperature imbalance

temperatures are tested and the peak temperatures and flow velocities at die outlet are compared in Table 4, where the values in parenthesis indicate the relative increases with respect to the values for the preceding inlet temperatures. It is found that the peak outlet temperature increases in proportional to the inlet temperature but the peak flow velocity saturates. Thus, the control of inlet temperature affects the temperature of extruded product, but its influence on the production speed is negligible. In fact, the inlet temperature gives rise to the effect on the final sectional shape of weather strip after forming, because the extruded product from the forming die experiences the thermal deformation to some extent during cooling down.

Figure 15a shows an example of twin dies which was proposed to increase the production capacity for a fixed number of extrusion forming machines. In other words, the production capacity becomes two times for each forming machine, provided that the extrusion forming is successful without causing any kind of production imperfection. However, unfortunately the test experiment at Hwaseung R&A encountered various kinds of problems, such as the imbalance between a pair of products and the imprecision of dimension and sectional shape. This kind of problem in extrusion forming using twin dies was suspected to be mostly caused by the imbalance of temperature distributions and flow velocity profiles between two dies in the head region. In order to examine why such an imbalance occurs, two kinds of imbalance conditions shown in Fig. 15a, b are considered. One is the imbalance of wall temperature in the head region, and the other is the imbalance of inlet flow velocity in front of the breaker. In case of the temperature imbalance, the normal temperature is set by 60 °C that is similar to the process temperature while $T+\Delta T$ on the right side is set by 70 °C. Meanwhile, for the flow velocity imbalance, the normal velocity is the same as the value given in Table 1 while the velocity on the left side is increased by two times (i.e., $v+\Delta v=2\times v$).

Figure 16 comparatively represents the temperature distributions of twin products at die exit. The case without temperature imbalance shows the exactly same distributions for both products, but the other case with the temperature imbalance leads to the apparent difference in the distributions. The symmetry and asymmetry at twin dies are also observed at the

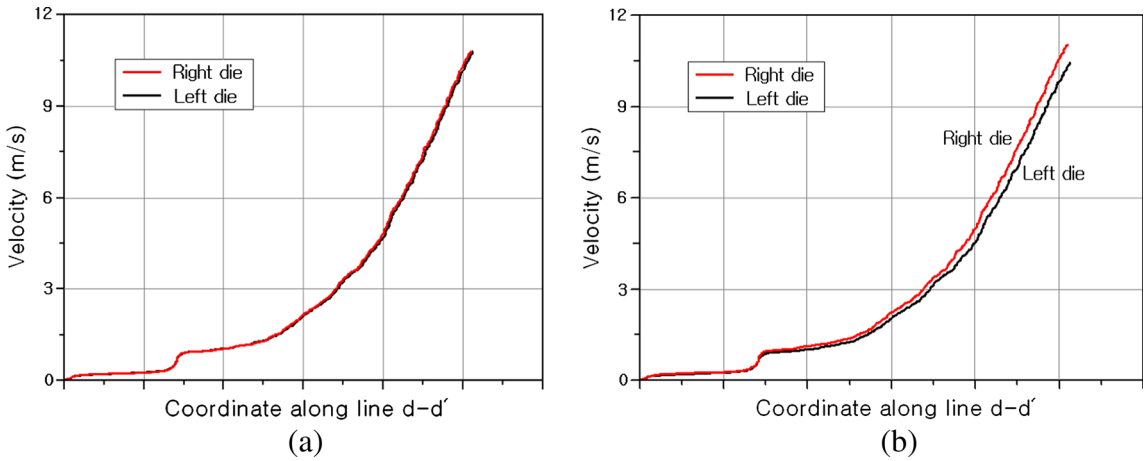

Fig. 17 Velocity distributions along lines *d*–*d*′: **a** without temperature imbalance, **b** with temperature imbalance

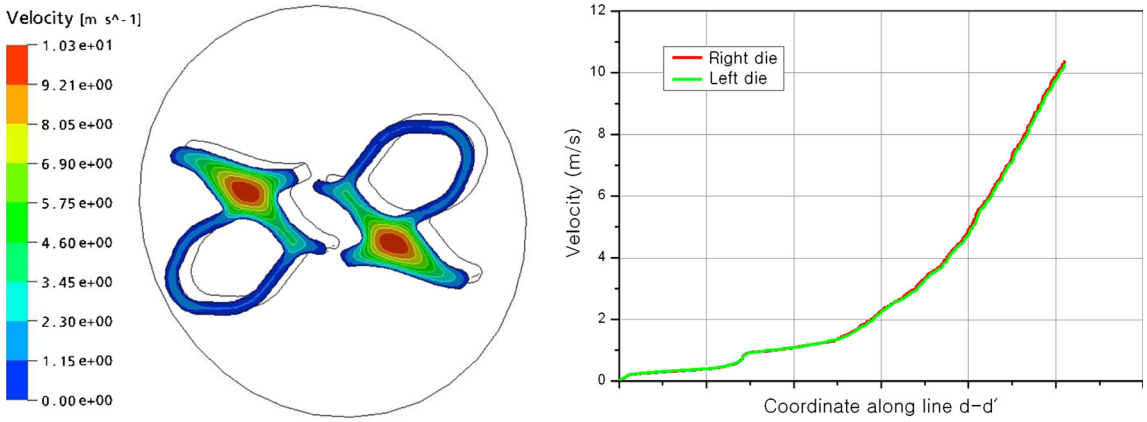

Fig. 18 To the velocity imbalance at inlet: **a** velocity profiles at die exit, **b** velocity distributions along lines *d*–*d*′

flow velocity profiles, as shown in Fig. 17. The flow velocity distributions at die exit are taken along two lines *d*–*d*′ shown in Fig. 16a which are identically defined for both dies. It is observed from Fig. 17b that the right die subject to higher wall temperature produces higher flow velocity than the left die. The maximum difference in velocities at two points *d*′ is found to be 0.67 m/s and it becomes 6.4 % of the peak velocity at the left die. It was observed from the experiment that a little difference in velocity profiles causes the remarkable imbalance of products, so this amount of difference is considered as a major difference. As a result, it is confirmed that the imbalance of wall temperature becomes a factor that causes an asymmetry in the thermal flow profiles at twin dies.

Next, the thermal flow analysis was performed for the twin dies subject to the imbalance of inlet flow velocity shown in Fig. 15b. This case does not lead to the asymmetry in the temperature distributions at die exit for both dies. Furthermore, there is no asymmetry in the flow velocity profiles at die exit, as shown in Fig. 18a. It can be clearly confirmed, from Fig. 18b, that the flow velocity distributions along two lines *d*–*d*′ are exactly the same. Thus, it has been confirmed that the imbalance of inlet flow velocity in front of the breaker plate does not cause the asymmetry in both the temperature and flow velocity distributions at die exit for twin dies. It is because, referring to Figs. 9 and 10 any asymmetry in the profile of the vortex flow in front of the breaker plate disappears while passing through a number of cylindrical holes that are formed in the breaker plate.

5 Conclusion

The thermal flow characteristics in the head region of extrusion forming process of weather strip were numerically investigated in this paper. The power-law viscosity model was employed to account for the effects of temperature and shear strain rate on the shear viscosity. The material parameters in the power-law model were determined based on the experimental data and the least square curve fitting. The free slip condition at the wall was chosen through the preliminary numerical experiment on the flow streamline after the breaker plate, the flow profile and the temperature distribution. The free slip condition predicts the peak flow velocity and the peak temperature at die exit which are close to the values that are measured from the real forming process.

Both the constant and power-law shear models lead to almost the same flow velocity profiles at die exit, but the both models show a noticeable difference in the temperature distributions. Furthermore, both models lead to the remarkable difference in the peak flow velocities and the peak temperatures. Based on the comparison with the measured temperature value and the improvement of cross-sectional flow uniformity at die exit, it has been justified that the power-law model is more appropriate to model the shear viscosity of melted rubber flow. Meanwhile, it was found from the parametric investigation with respect to the inlet temperature that the production speed is not greatly influenced by the inlet temperature.

According to the thermal flow analysis to examine the asymmetry in temperature and flow velocity distributions for twin dies, the following observations are drawn. The imbalance of wall temperature in the head region is a critical factor causing the asymmetry in the extrusion forming of weather strip using twin dies. But, the imbalance of inlet flow velocity does not produce a noticeable asymmetry in the temperature and flow velocity profiles because the flow imbalance is to be recovered while passing through the breaker plate.

Acknowledgments This work was supported by the Hongik University new faculty research support fund.

References

1. Cho JR, Han KC, Kim JS, Lee SB, Lim OK (2012) Fatigue life prediction and optimum topology design of EPDM weather strip. Fin Elem Anal Des 60:57–63
2. Kim JK, Park SH, Hwang SH (2000) Study on rear door fixed glass weather-strip for automobile using EPDM/polypropylene blend. Elastomer 35(1):115–121
3. Stenti A, Moens D, Sas P, Desmet W (2008) Low-frequency dynamic analysis of automotive door weather-strip seals. Mech Syst Sig Proc 22(5):1248–1260
4. Ha YS, Cho JR, Kim TH, Kim JH (2008) Finite element analysis of rubber extrusion forming process for automobile weather strip. J Mater Process Technol 201:168–173
5. Covas JA, Carneiro OS, Brito AM (1991) Designing extrusion dies for thermoplastics. J Elastomer Plast 23(3):218–238
6. Na S (1998) Modeling and optimum shape design of polymer extrusion die, Ph.D Thesis, KAIST, Korea
7. Wu CY, Hsu YC (2002) Optimal shape design of an extrusion die using polynomial networks and genetic algorithms. Int J Adv Manuf Technol 19:79–87
8. Pilani R, Narasimhan K, Maiti SK, Singh UP, Date PP (2000) A hybrid intelligent systems approach for die design in sheet metal forming. Int Adv Manuf Technol 16:370–375
9. Reddy JN, Gartling DK (1994) The finite element method in heat transfer and fluid dynamics. CRC Press, New York
10. Gerhart PM, Gross RJ, Hochstein JI (1992) Fundamentals of fluid mechanics. Addison-Wesley Publishing Company, Wiley, Chichester
11. Arroyo M, Lopez-Manchado MA, Herreto N (2003) Organomontmorillonite as substitute of carbon black in natural rubber compounds. Polymer 44(8):2447–2453
12. Bathe KJ (1996) Finite element procedure. Prentice-Hall, New Jersey
13. Ansys (2013) User's manual of CFX. Ansys Inc, USA
14. Lin SY (1999) Investigation of die-workpiece interface friction with lubrication during the upsetting process. Int Adv Manuf Technol 15:666–673